**Atmospheric
Chemistry
and Physics
Discussions**

High resolution VHF radar measurements of tropopause structure and variability at Davis, Antarctica (69° S, 78° E)

S. P. Alexander, D. J. Murphy, and A. R. Klekociuk

Australian Antarctic Division, Kingston, Tasmania, Australia

Correspondence to: S. P. Alexander (simon.alexander@aad.gov.au)

Discussion Paper | Discussion Paper | Discussion Paper | Discussion Paper

ACPD

12, 26173–26205, 2012

Antarctic radar tropopause

S. P. Alexander et al.

Title Page

Abstract	Introduction
Conclusions	References
Tables	Figures

|◄ | ►|

◄ | ►

Back | Close

Full Screen / Esc

Printer-friendly Version

Interactive Discussion

Abstract

Two years of VHF radar echo power observations are used to examine the structure and variability of the tropopause at Davis, Antarctica. Co-located radiosonde and ozonesonde launches provide data with which to calculate the thermal (lapse-rate) and
5 chemical tropopauses at Davis. The dynamically-controlled radar tropopause can be used as a definition of the Antarctic tropopause throughout the year under all meteorological conditions. During the extended summer period of December–April (DJFMA) inclusive, radar tropopauses are (0.2 ± 0.4) km lower than co-located radiosonde thermal tropopauses and during the extended winter period of June–October (JJASO) inclu-
10 sive, the radar tropopauses are (0.8 ± 1.0) km lower. The radar and ozone tropopauses both show a decrease in altitude under increasingly strong cyclonic conditions. During strong JJASO cyclonic conditions, there are large (several km) differences between radiosonde lapse-rate tropopause altitudes and radar tropopause altitudes. However, the radar tropopause altitude closely corresponds to the altitude of the 2 PVU sur-
15 face (where $1\,\mathrm{PVU} = 10^6\,\mathrm{m^2\,s^{-1}\,K\,kg^{-1}}$) for both cyclonic and anticyclonic conditions. The monthly mean occurrence frequency of tropopause folds is investigated using the radar tropopause and is about 1 per month during DJFMA and about 3 per month during JJASO. The power spectrum of the Davis radar tropopause altitude indicates its influence by the passage of inertio-gravity waves. The higher power spectral density
20 during JJASO also indicates an increase in gravity wave activity during this time.

1 Introduction

The upper troposphere and lower stratosphere (UTLS) is the atmospheric region within a few kilometers of the tropopause. It is a highly coupled region, where radiation, dynamics, clouds and chemical processes control its structure on a wide variety of spa-
25 tial and temporal scales (Gettelman et al., 2011). In the extratropics, baroclinic waves and atmospheric fronts enable stratosphere–troposphere exchange (STE), whereby air

Title Page

Abstract	Introduction
Conclusions	References
Tables	Figures

◄◄ ►►

◄ ►

Back Close

Full Screen / Esc

Printer-friendly Version

Interactive Discussion

masses irreversibly move across the tropopause. These air masses may be followed using dynamical or chemical tracers (Hocking et al., 2007; Sprenger et al., 2003; Pan et al., 2009). The extra-tropical transition layer is the region of atmosphere where the air shows a mix of stratospheric and tropospheric properties, and is often studied using vertically-resolved trace gas profiles such as ozone and water vapour (e.g. Heggelin et al., 2009). Synoptic-scale and mesoscale processes are important for extra-tropical STE (Stohl et al., 2003), which occurs during tropopause folding (Sprenger et al., 2003; Reid and Vaughan, 2004), cut-off lows (Sprenger et al., 2007; Wernli and Sprenger, 2007) and streamers (Vaughan and Timmis, 1998). Individual tropopause folds and cut-off lows can occur over wide latitudinal extent (Sprenger et al., 2003) allowing the transfer of large amounts of air between the stratosphere and troposphere. Tropopause folds are of interest because of their role in frontogenesis, initiation of severe weather and for the STE which occurs (Sprenger et al. (2003) and references therein).

The tropopause itself is often defined in the polar regions using radiosonde data which provide the lapse rate (thermal) tropopause. However, during the winter and spring, the temperature often continues to decrease with altitude throughout the UTLS and may not reach the gradient threshold required by the lapse-rate tropopause definition criteria. This ill-defined lapse-rate tropopause illustrates that the thermal criterion is often not suitable for Antarctic winter or spring (Zängl and Hoinka, 2001). One possibility is to define the tropopause chemically, such as sharp, step-like increases in the vertical profile of ozone mixing ratio. The ozone tropopause is clearly defined even during the Antarctic winter and spring (Tomikawa et al., 2009). Alternatively, a dynamical tropopause based on a specified potential vorticity (PV) surface calculated from reanalysis fields may be used (Holton et al., 1995). A value of $2\,\text{PVU}$ (where $1\,\text{PVU} = 10^6\,\text{m}^2\,\text{s}^{-1}\,\text{K}\,\text{kg}^{-1}$) is often chosen to indicate the tropopause level (Hoskins et al., 1985). These different tropopause definitions are related to each other via vertical gradients in static stability and horizontal vorticity gradients (Gettelman et al., 2011). Global climatologies of tropopause altitude have blended the dynamical and thermal tropopause definitions across the sub-tropical region (Wilcox et al., 2011).

Title Page

Abstract | Introduction

Conclusions | References

Tables | Figures

◄ | ►►

◄ | ►

Back | Close

Full Screen / Esc

Printer-friendly Version

Interactive Discussion

One way to investigate the detailed structure of the tropopause is through the use of echo return power from Very High Frequency (VHF) radars. These radars are capable of continuous monitoring (Gage and Green, 1979, 1982) with a much higher temporal resolution than radiosonde, ozonesonde or satellite observations, although they are limited to a few locations globally. The radar tropopause is deduced from the local maximum in power observed directly above it in the lowermost stratosphere (Gage and Green, 1979; Vaughan et al., 1995; Hooper et al., 2008). Observations of the radar tropopause with temporal resolutions on the order of a few hours have revealed its rich structure and altitudinal variability on sub-diurnal time-scales (Nastrom et al., 1989). The Arctic VHF radar tropopause altitude has been investigated above Svalbard (78° N, 16° E) (Hall et al., 2009, 2011) and Kiruna (68° N, 21° E) (Hooper and Arvelius, 2000). A VHF radar was deployed at Wasa (73° S, 13° W) during the Antarctic summer of 2007–08, which provided wind and turbulence observations up to the lower stratosphere. Results from this radar were used in fine-scale modelling case studies to investigate gravity waves seen in the radar data and were shown to be generated by nearby topography (Valkonen et al., 2010; Arnault and Kirkwood, 2012).

Using two years of VHF radar echo power observations from Davis, Antarctica, we present the high-resolution characteristics of the Antarctic tropopause. Differences between co-located radar, radiosonde and ozonesonde definitions of tropopause altitude are quantified. We demonstrate the robustness of the Antarctic VHF radar tropopause in both summer and winter even during cyclonic meteorological conditions. We quantify the seasonal variation in the occurrence frequency of tropopause folds and demonstrate the influence of gravity wave activity on the radar tropopause altitude.

2 Data

The VHF radar located at Davis, Antarctica (69° S, 78° E) operates at 55 MHz. A Doppler beam steering experiment was run between August 2009 and October 2011. We use the two years of data from September 2009–August 2011 inclusive. Details

of the experimental setup relevant to this study are given in Table 1; further details of the system are presented by Morris et al. (2006). While the experiment also used off-vertical beams to provide radial velocities and thus the three-dimensional wind components, we do not discuss the wind data here because it is generally restricted

5 to the lower troposphere. The echo power received $P_{radar}(z)$ is proportional to the square of the vertical gradient of the refractive index n. The generalized refractive index $M \propto \partial n / \partial z$ thus $P_{radar}(z) \propto M^2$ (Gage et al., 1981). Humidity can be neglected in the upper troposphere and lower stratosphere (UTLS) so that (Doviak and Zrnic, 1984):

$$M = -77.6 \times 10^{-6} \frac{p}{T} \frac{\partial \ln \theta}{\partial z} \qquad (1)$$

10 where p is pressure, T temperature, θ potential temperature and z altitude. M is proportional to the vertical gradient of $\ln \theta$ and this relationship allows the detection of the tropopause (and also changes in static stability associated with frontal passages) by the radar backscattered power (Tsuda et al., 1988; Nastrom et al., 1989; May et al., 1991; Lucas et al., 2001). The upper troposphere temperature gradient is usually close

15 to the dry adiabatic lapse rate, thus the static stability ($\propto \partial \ln \theta / \partial z$) is small and the radar's echo returns are low. Due to the rapid increase in static stability upon the transition into the stratosphere, the radar detects a local maximum in echo power directly above the tropopause. The radar tropopause is thus defined as the altitude of the maximum vertical gradient of the echo power (Gage and Green, 1979; Vaughan et al.,

20 1995). This use of vertical power gradients avoids reliance on the absolute echo power of the radar.

Some averaging of the original 8 min temporal resolution power profiles is necessary because by differentiating the power, the results have a greater sensitivity to noise. To minimise this noise, the data are averaged into 2 h blocks and then smoothed vertically

25 using a 3-point running mean to form a power profile $P_{radar}(z)$, similar to the method of Hooper and Arvelius (2000). Local maxima in the vertical power $P_{radar}(z)$ gradient are flagged as a possible tropopause at this z if the range-weighted power $z^2 P_{radar}(z)$ is greater than the mean range-weighted power values from -900 m to 0 m (below, i.e.

three range gates) and less than the mean range-weighted power values from 0 m to +900 m above. The altitude of the radar tropopause z_{radar} is the altitude of the largest maximum gradient of $P_{radar}(z)$ satisfying these conditions. A few isolated z_{radar} outliers are removed by constructing a 24 h running mean time series and removing those z_{radar}
5 which are more than 2 standard deviations outside this running mean.

Radiosondes are launched either daily or twice-daily at Davis. The radiosonde lapse rate (thermal) tropopause z_{sonde} is calculated from full resolution ($\sim$ 5 m) profiles binned to 100 m in the standard manner, specifically it is the lowest altitude (above 500 hPa) at which the temperature lapse rate falls below $2 \, K \, km^{-1}$ and the average lapse rate within
10 2 km above this altitude does not exceed $2 \, K \, km^{-1}$ (World Meteorological Organization, 1957).

Ozone is used as the tracer to define the chemical gradient tropopause and we follow the ozone tropopause z_{ozone} criteria of Bethan et al. (1996), modified for Antarctic conditions by Tomikawa et al. (2009). Specifically, z_{ozone} is the lowest altitude at
15 which the vertical ozone mixing ratio gradient exceeds $60 \, ppbv \, km^{-1}$; the mixing ratio > 80 ppbv and the mixing ratio at 500–1500 m above z_{ozone} is > 110 ppbv. Ozonesondes are launched at Davis on average once a week during the ozone hole season (June–October), but about monthly for the remainder of the year. Due to the much lower quantity of ozonesonde data compared with radiosonde and radar data, ozonesonde
20 data over the nine years from February 2003 until March 2012 are used to provide sufficient ozone tropopause information for comparisions with relative vorticity. The total number of ozone launches during this period, as well as that during the September 2009–August 2011 period when radar data is available, is shown in Fig. 1. The more frequent ozonesonde launches during the ozone-hole season are clearly visible.
25 The 2 PVU level of the potential vorticity provided by the European Centre for Medium-Range Weather Forecasts (ECMWF) Reanalysis-Interim (ERA-Interim) (Dee et al., 2011) dataset is used as the dynamical tropopause and in geometric altitude this is referred to as $z_{2\,PVU}$.

The ozone, thermal and radar tropopauses are illustrated using data on 19 March 2010 in Fig. 2 and are at 10.4 km, 10.2 km and 9.8 km, respectively. Temperature is measured by the ozonesonde, while the radar echo power profile is that averaged over the two hours prior to the ozonesonde launch (the two-hour average echo power

5 profile during the flight did not provide a radar tropopause). On this day, the thermal tropopause is clearly defined with a distinct change in the temperature profile visible at the tropopause, as is usually observed in the polar summer (Randel and Wu, 2010). Both the z_{ozone} and z_{radar} clearly correspond to large vertical gradients in ozone mixing ratio and echo power, respectively. There are some small differences in the altitudes

10 between the three tropopauses which are due to their different definitions.

Using the standard radiosonde dynamical quantities, Eq. (1) may be calculated using radiosonde data to produce M_{sonde} (neglecting humidity) which can then be compared with the radar echo power returns. Examples of this are illustrated for 21 September 2009 in Fig. 3a and 26 March 2010 in Fig. 3b, along with profiles of $P_{radar}(z)$ and

15 $z^2 P_{radar}(z)$. The profiles are smoothed vertically over three range gates as per the radar tropopause-detection algorithm. The sharp increase in M_{sonde} is co-incident with that of $z^2 P_{radar}(z)$.

3 Results

3.1 Fine-scale structure of the radar tropopause

20 The radar power P_{radar} is illustrated in Fig. 4 for a representative winter and summer month (September 2009 and March 2010, respectively), along with z_{radar}, z_{sonde}, z_{ozone} and $z_{2\,PVU}$. For reasons related to the seasonal variability in the tropopause structure (discussed below), the extended winter season is defined as the months June–October inclusive (referred to as JJASO), and the extended summer season as December–April

25 inclusive (DJFMA). The tropopause altitude varies on a multitude of time scales. The z_{sonde} closely follows z_{radar} during DJFMA months (Fig. 4b). Differences between z_{radar}

and z_{sonde} during JJASO of a few kilometres are sometimes apparent (e.g. 25 September, Fig. 4a). During September 2009 there are days with weak P_{radar} gradients, for example 23–27 September, although a z_{radar} is usually still detectable and closely follows z_{2PVU}.

5   Sudden increases in z_{radar} (e.g. 17 September 2009) are reminiscent of the tropopause folds associated with stratospheric intrusions of ozone into the troposphere identified in the Northern Hemisphere (Hocking et al., 2007). Events such as this will be classified as tropopause folds below. Weekly ozone launches at Davis during September 2009 show that z_{ozone} is slightly higher than z_{radar}. During March 2010 the z_{radar}
10 and z_{sonde} are nearly co-incident in height, while on some days z_{2PVU} is slightly lower than z_{radar}.

    The seasonally-varying strength of the radar tropopause relative radar power P_{rel} is illustrated in Fig. 5. The maximum power is 600–900 m higher than z_{radar} throughout the year. There is a seasonal cycle in the UTLS P_{rel}, with the maximum occurring in
15 late summer and early autumn, while the minimum is from late winter until early spring. The vertical gradient in UTLS power is also strongest during late summer and weakest during late winter.

3.2   Comparisons between different tropopause definitions at Davis

Tropopause data are combined for the two-year analysis period into monthly mean
20 radar tropopause altitude z_r, radiosonde lapse rate tropopause altitude z_s, ozone tropopause z_o and radiosonde horizontal wind speed V_h in Fig. 6. The altitude of z_s exhibits an annual cycle, with maxima in late winter and early spring. The z_r annual cycle is smaller than z_s. Both mean tropopauses are about 8.5 km altitude during late summer, but the winter monthly mean z_r is around 9.0 km compared with around 10.0 km
25 for z_s. The vertical bars in Fig. 6 indicate the standard deviations: much larger variability in both z_r and z_s is evident during winter than during summer. Horizontal wind speed is largest at the tropopause (except during winter where the lower levels of the stratospheric polar night jet are seen). The monthly mean V_h at the tropopause vary

from around $15\,\mathrm{m\,s}^{-1}$ in summer to around $20\,\mathrm{m\,s}^{-1}$ in winter. The monthly mean z_s is above the peak wind speed in winter while z_r is centred on the peak wind speed (except in August where the tropopause peak in wind speed is ill-defined). The winter-time monthly mean z_o are lower than z_s but above z_r. The anomalous January z_o is due to a single ozonesonde launched during this month at the time when z_r was also at its highest point (not shown, but similar to the one ozonesonde launched in March 2010 with respect to z_{radar}, see Fig. 4b). Based on these results with the clear seasonal changes in tropopause properties, summer is defined to be December–April inclusive (DJFMA) and winter June–October (JJASO) inclusive.

The histogram frequency distribution of the differences in altitude between z_{radar} and z_{sonde} for DJFMA and JJASO are displayed in Fig. 7a. The DJFMA distribution is approximately Gaussian, with a mean (and standard deviation) difference of $(-0.3 \pm 0.4)\,\mathrm{km}$. The mean difference during JJASO is much larger than during DJFMA $(-0.8 \pm 1.0)\,\mathrm{km}$, with nearly all of the z_{radar} lower than z_{sonde}. In contrast, the DJFMA and JJASO distribution between z_{radar} and $z_{\mathrm{2\,PVU}}$ is similar (Fig. 7b). The z_{radar} is 0.2–0.3 km higher than $z_{\mathrm{2\,PVU}}$ during both seasons. Figure 7b indicates the closer relation between JJASO z_{radar} and the dynamical state of the UTLS (as represented by $z_{\mathrm{2\,PVU}}$) than the relation between JJASO z_{radar} and the thermal state of the UTLS (i.e. z_{sonde}).

The M_{sonde} vertical profile may be used to calculate the radiosonde's refractive index tropopause z_{M^2} in a similar manner to that for z_{radar}. The z_{M^2} and z_{radar} should agree closely because they are measuring the same atmospheric dynamical properties (excluding humidity effects). Figure 7c shows the differences are similar and are $(-0.4 \pm 0.4)\,\mathrm{km}$ in DJFMA and $(-0.6 \pm 0.8)\,\mathrm{km}$ in JJASO.

Differing tropopause-relative structures of radiosonde N^2 occur as a consequence of the differences between z_{sonde} and z_{radar}. Figure 8 illustrates these differences, where N^2 values at heights measured relative to z_{sonde} and z_{radar} are averaged for both seasons. During DJFMA the strong tropopause inversion layer (TIL) is evident in both z_{sonde}- and z_{radar}-based co-ordinates with a similar magnitude, although the z_{radar}-based TIL has a slightly steeper gradient. There are larger differences in N^2 during

JJASO (Fig. 8b) due to the large JJASO differences. In the z_{sonde}-based co-ordinates, the sharp, discontinuous TIL structure is evident (Birner, 2006; Tomikawa et al., 2009), which becomes smoothed out in the z_{radar}-based co-ordinates. Furthermore, there is no local maximum in N^2 just above the z_{radar} tropopause and there is a much less stable upper tropopause in the z_{radar}-based co-ordinates.

3.3 Tropopause relation to mesoscale meteorology

The meteorological effect on tropopause heights are investigated by using the vertical component of relative vorticity ζ from the ERA-Interim reanalysis data (Dee et al., 2011) at the near-tropopause level of 200 hPa. This pressure level is the same as that used by Randel et al. (2007) and Randel and Wu (2010) and will allow direct comparisons to be made below. (Use of other pressure levels around 200 hPa reveal similar features as those to be illustrated below.) Radiosonde and radar tropopause heights for DJFMA are plotted in Fig. 9a as a function of ζ. The tropopause height is lower when there is negative vorticity and higher when there is positive vorticity (negative vorticity is associated with cyclonic conditions in the Southern Hemisphere). The difference between z_{sonde} and z_{radar} is similar during both cyclonic and anticylonic conditions. The February 2003–March 2012 z_{ozone} are also shown in Fig. 9a and generally match the tropopause altitudes using the other two definitions.

Increasingly large differences between z_{sonde} and z_{radar} occur under increasingly strong JJASO cyclonic conditions (Fig. 9c), explaining the meteorological origin of the differences between z_{sonde} and z_{radar} (Figs. 4a and 7a). The JJASO z_{radar} and z_{ozone} more closely follow the summertime vorticity-dependent structure than z_{sonde} does. This indicates that the JJASO z_{radar} and z_{ozone} are more closely aligned with mesoscale UTLS dynamical processes during the polar winter than z_{sonde}. Both the DJFMA and JJASO ζ distributions (Figs. 9b and 9d, respectively) indicate the high latitude preference for cyclonic activity, consistent with Northern Hemisphere results (Randel et al., 2007).

Antarctic radar tropopause

S. P. Alexander et al.

Title Page

Abstract	Introduction
Conclusions	References
Tables	Figures

| ◄◄ | ►► |
| ◄ | ► |

| Back | Close |

Full Screen / Esc

Printer-friendly Version

Interactive Discussion

3.4 Tropopause folds

Folds are identified in radar echo power time series by a gradual decrease in tropopause altitude followed by a sudden increase as the tropopause reforms at a higher altitude (Nastrom et al., 1989). Other radar parameters may also be used as
5 supplementary diagnostics of tropopause folds. These include horizontal wind shear and spectral width (Vaughan and Worthington, 2000; Reid and Vaughan, 2004), horizontal wind speeds (Rao et al., 2008) and aspect ratio (Caccia et al., 2000; Bertin et al., 2001). However, this tropopause detection algorithm only uses the echo power because radar horizontal winds are unavailable in the UTLS.
10 Tropopause folds are defined at time t where the median increase in z_{radar} for the following six hours is at least five range gates (1200 m) and the $z_{radar}(t) < 8.0$ km. These limits may be varied without too much change in the number of fold detections. However, a six-hourly median increase in z_{radar} of more than three range gates avoids mis-assignment of fold where the tropopause height variation is actually due to real,
15 but small-scale tropopause variability.

Using this tropopause fold detection algorithm, folds are classified as occurring on 3, 17 and 22 September 2009 and on 29 March 2010 (see Fig. 4). In all of these cases, the descent of the layer of increased $P(z)$ (and thus z_{radar}) is evident. The increased $P(z)$ layer may be followed by eye down below 6 km, although the tropopause-detection
20 algorithm identifies z_{radar} reforming above ~ 8 km as the lower $P(z)$ layer continues to descend.

The monthly mean number of tropopause folds for September 2009–August 2011 is presented in Fig. 10. While this two-year dataset may be too short to provide a climatology of monthly folds, the difference between DJFMA and JJASO is clearly apparent.
25 The average number of folds during DJFMA is 1.1 per month and during JJASO nearly triples to 2.9 per month.

3.5 Tropopause altitude power spectra

Observations of gravity waves at various locations and altitudes lead to the development of a theory whereby the frequency spectra of horizontal wind velocity and temperature are $\propto \omega^{-p}$, where ω is frequency and p is the gradient of the spectrum (Fritts and VanZandt, 1993). The p is typically $\frac{5}{3}$, although it can vary between about 1 and 2 (Fritts and Alexander, 2003). The tropopause altitude is likely affected by temperature and wind fluctuations due to the passage of inertia-gravity waves. While two dimensional turbulence is a possible explanation of the horizontal wavenumber power law in the lower stratosphere (e.g. Gage, 1979), radar results demonstrated that it is gravity waves rather than two dimensional turbulent mixing which explains the observed wind perturbations (Vincent and Eckermann, 1990). Therefore it is reasonable to suppose that the perturbations observed in tropopause altitude at Davis are also due to these waves.

To investigate these effects on tropopause altitude, the z_{radar} power spectra are calculated in 24 h blocks, stepped forward by 12 h. The composite results for JJASO 2010 and DJFMA 2010/11 are shown in Fig. 11 (other seasons are similar). The JJASO power spectral density (PSD) is twice that of the DJFMA PSD over the 4–24 h ground-based periods τ_g, indicating that there is greater JJASO variability in tropopause altitude on these time scales and thus more gravity wave activity during JJASO. During both seasons at $\tau_g = 6$–24 h $p \sim 2$ while a noise floor is evidently being approached at $\tau_g < 6$ h as the spectra flatten during both seasons.

4 Discussion

The Davis VHF radar is able to continously monitor the tropopause, allowing quantification of differences between the radar and other tropopause definitions. Following an analysis of radiosonde thermal tropopause data, Zängl and Hoinka (2001) concluded that the thermal tropopause criterion is not appropriate for polar winter, where

Title Page

Abstract | Introduction

Conclusions | References

Tables | Figures

◄◄ | ►►

◄ | ►

Back | Close

Full Screen / Esc

Printer-friendly Version

Interactive Discussion

temperatures may keep decreasing into the stratosphere with no temperature inversion. Zängl and Hoinka (2001) noted that other than vertically-resolved trace gas profiles such as ozone, there appeared no alternative but to use a potential vorticity (PV) based tropopause during polar winter, yet this still has limitations such as defining the appropriate PV level. Our results of JJASO-time tropopause heights in cyclonic and anti-cyclonic conditions shows a steady decrease in both z_{radar} and z_{ozone} for increasingly strong cyclones (Fig. 9), thus we suggest the use of z_{radar} as another dynamical definition of the polar tropopause which is valid year-round under all meteorological conditions.

Wilcox et al. (2011) used the 2 PVU surface from ERA-Interim data to construct an Antarctic-wide tropopause climatology, although they questioned the significance of an Antarctic wintertime dynamical tropopause definition. Figures 4 and 7b reveal the close correspondence between the radar tropopause and the height of the 2 PVU surface. This indicates that above Davis at least, the 2 PVU surface appears a valid choice to mark the wintertime dynamical tropopause.

The post-summer solstice maximum and the post-winter solstice minimum Davis radar tropopause relative power (Fig. 5) are consistent with the timing of Antarctic-wide radiosonde and satellite measurements of maxima in static stability, UTLS water vapour and the strength of the polar tropopause inversion layer (Tomikawa et al., 2009; Randel and Wu, 2010).

Climatological means in traditional sea-level pressure based co-ordinates tend to smear out details of the UTLS structure, such as the TIL identified using a lapse-rate tropopause relative co-ordinate system (Birner et al., 2002; Birner, 2006; Randel et al., 2007), and cloud-top height (Pan and Munchak, 2011). Thus the z_{radar} relative profiles of radiosonde N^2 result in a smearing out of the details, and the vanishing of the TIL and of the maximum in N^2 directly above the tropopause during JJASO (Fig. 8b). The JJASO structure of N^2 in radar tropopause based co-ordinates is similar to N^2 relative to the dynamical (PV) tropopause during cyclonic conditions (Wirth, 2003), indicating the effects that meteorological disturbances have on z_{radar}. The re-

Title Page

Abstract | Introduction

Conclusions | References

Tables | Figures

◄ | ►

◄ | ►

Back | Close

Full Screen / Esc

Printer-friendly Version

Interactive Discussion

lationship between ζ and z_{radar} compared with that between ζ and z_{sonde} illustrates the dynamically-controlled nature of z_{radar}. It also illustrates that z_{ozone} is dynamically controlled, which follows given that on synoptic time-scales the ozone mixing ratio is approximately materially conserved (Wirth, 2000).

Randel and Wu (2010) discussed Arctic average summertime GPS radio occultation temperature lapse-rate tropopause heights as a function of ζ and showed the same relationship as that observed with radiosonde and radar at Davis. During the Northern Hemisphere mid-latitude (30°–60° N) winter, the lapse-rate tropopause decreased with altitude for weaker anticyclonic activity and remained relatively constant (< 0.5 km variability) under cyclonic conditions (Randel et al., 2007). The lapse-rate tropopause altitude at Davis is also approximately constant for cyclonic conditions (Fig. 9b). This separation of the altitudes of the thermal and dynamical tropopause during strongly cyclonic conditions was modelled by Wirth (2000, 2001). Large differences between ozone and thermal tropopauses reported by Bethan et al. (1996) were associated with indefinite thermal tropopauses and cyclonic conditions, as they are at Davis between thermal and dynamical tropopauses. The DJFMA results at 69° S (Fig. 9a) are in good agreement with the 70°–90° N summertime GPS lapse-rate tropopause height relationship with ζ (Randel and Wu, 2010).

The JJASO peak in the number of tropopause folds seen at Davis is similar to that observed by radar in northern Sweden (Rao et al., 2008) and more generally in global ECMWF data (Sprenger et al., 2003) in the high latitudes. The descent of z_{radar} often co-incides with large differences from the altitude of z_{sonde} (Fig. 4a), thus the folds are occurring during strongly cyclonic conditions (Fig. 9b). The region from 60° S to the Antarctic coastline at 60° E–100° E (encompassing Davis) has the highest percentage of tropopause folds during winter poleward of 60° S (Sprenger et al., 2003). This was attributed to the co-incident location of the climatological maximum of moving cyclones.

The gradient of the z_{radar} power spectra is within the range of that expected if it were due to gravity wave activity, which indicates that the Davis radar tropopause altitude is influenced on sub-diurnal time scales by gravity wave activity. It is likely that z_{radar}

is influenced by both horizontal and vertical motions, although further analysis of this must await the availability of Antarctic UTLS radar winds. There is a slight ($\sim 5\,\mathrm{m\,s^{-1}}$) increase in the strength of the monthly mean horizontal wind speed at the tropopause (8–10 km altitude) during JJASO (Fig. 6a), when the power spectral density doubles (Fig. 11).

The increased level of UTLS gravity wave activity and variability in z_{radar} during JJASO provides further observational support for seasonally-varying (JJASO peak) UTLS gravity wave activity seen in a high-resolution model in the mid- to high south-ern latitudes (Sato et al., 2009) and suggests seasonal changes in source strength. Gravity waves observed with the Davis Rayleigh lidar in the upper stratosphere and lower mesosphere (USLM) with $\tau_g > 2\,\mathrm{h}$ and vertical wavelengths between 4 km and 20 km also show a seasonal cycle with largest activity in winter and weaker activity at the equinoxes (Alexander et al., 2011), although waves in the USLM have not neces-sarily propagated vertically from source regions around Davis. Alexander et al. (2011) demonstrated that not all of this winter increase in USLM gravity wave activity could be related to Doppler shifting by the stronger winter wind speeds, and that some was likely related to changes in source strength and variability. The larger JJASO power spectral density of the tropopause altitude seen in Fig. 11 is likely due in part to an in-creased source strength. There is no peak in the tropopause power spectral density at the diurnal frequency (or its sub-diurnal harmonics) in contrast with radar observations of the tropical tropopause (Yamamoto et al., 2003), indicating negligible diurnal forcing effects on the polar radar tropopause altitude.

5 Conclusions

Echo power data from the VHF radar located at Davis, Antarctica for the period September 2009–August 2011 inclusive are used to characterise the seasonal struc-ture and variability of the radar tropopause. The radar has the ability to continuously

monitor with high temporal resolution a dynamical tropopause, including during polar winter under cyclonic and anti-cyclonic conditions.

Co-located radiosonde and ozonesonde profiles provide the data for calculation of the thermal (lapse-rate) and chemical tropopauses at Davis. Radar tropopauses are (0.2 ± 0.4) km lower than radiosonde tropopauses during DJFMA and are (0.8 ± 1.0) km lower during JJASO. The times of largest differences between the radiosonde and radar definitions of the tropopause altitude occur during JJASO cyclonic activity. The ozone tropopause and the radar tropopause altitudes both steadily decrease with increasingly strong cyclonic activity, unlike the radiosonde tropopause altitudes which are nearly constant during increasingly strong cyclonic conditions. Both the radar tropopause and ozone tropopause are dynamically controlled. The altitude of the radar tropopause closely corresponds to the altitude of the 2 PVU surface for both cyclonic and anticyclonic conditions during DJFMA and JJASO.

The frequency of tropopause folds increases from about one per month during DJFMA to about three per month during JJASO. This is indicative of an increase in STE events during the ozone-hole season. The gradient of the power spectrum of the radar tropopause altitude is within the range expected if it were due to a gravity wave spectrum. This indicates that horizontal velocity and temperature perturbations due to gravity waves likely influence the radar tropopause altitude.The higher power spectral density during JJASO indicates a seasonal increase in tropospheric gravity wave activity with a JJASO maximum. Given the upper tropospheric frontogenesis, cyclogenesis and STE implications of tropopause folds (Sprenger et al., 2003), a more detailed investigation of these folds at Davis may shed further light on STE processes in the high southern latitudes.

References

Alexander, S. P., Klekociuk, A. R., and Murphy, D. M.: Rayleigh lidar observations of gravity wave activity in the winter upper stratosphere and lower mesosphere above Davis, Antarctica (69° S, 78° E), J. Geophys. Res., 116, D13109, doi:10.1029/2010JD015164, 2011. 26187

5 Arnault, J. and Kirkwood, S.: Dynamical influence of gravity waves generated by the Vestfjella Mountains in Antarctica: radar observations, fine-scale modelling and kinetic energy budget analysis, Tellus A, 64, 17261, doi:10.3402/tellusa.v64i0.17261, 2012. 26176

Bertin, F., Campistron, B., Caccia, J. L., and Wilson, R.: Mixing processes in a tropopause fold observed by a network of ST radar and lidar, Ann. Geophys., 19, 953–963,

10 doi:10.5194/angeo-19-953-2001, 2001. 26183

Bethan, S., Vaughan, G., and Reid, S. J.: A comparison of ozone and thermal tropopause heights and the impact of tropopause definition on quantifying the ozone content of the troposphere, Q. J. Roy. Meteorol. Soc., 122, 929–944, 1996. 26178, 26186

Birner, T.: Fine-scale structure of the extratropical tropopause region, J. Geophys. Res., 111,

15 D04104, doi:10.1029/2005JD006301, 2006. 26182, 26185

Birner, T., Dörnbrack, A., and Schumann, U.: How sharp is the tropopause at midlatitudes?, Geophys. Res. Lett., 29, 1700, doi:10.1029/2002GL015142, 2002. 26185

Caccia, J. L., Bertin, F., Campistron, B., Klaus, V., Pointin, Y., van Baelen, J., and Wilson, R.: Cut-off low monitoring by the French VHF-ST radar network during the ESTIME campaign, J.

20 Atmos. Sol. Terr. Phys., 62, 639–651, 2000. 26183

Dee, D. P., Uppala, S. M., Simmons, A. J., Berrisford, P., Poli, P., Kobayashi, S., Andrae, U., Balmaseda, M. A., Balsamo, G., Bauer, P., Bechtold, P., Beljaars, A. C. M., van de Berg, L., Bidlot, J., Bormann, N., Delsol, C., Dragani, R., Fuentes, M., Geer, A. J., Haimberger, L., Healy, S. B. Hersbach, H., Holm, E. V., Isaksen, L., Kallberg, P., Kohler, M., Matricardi,

25 M., McNally, A. P., Monge-Sanz, B. M., Morcrette, J.-J., Park, B.-K., Peubey, C., de Rosnay, P., Tavolato, C. Thepaut, J.-N., and Vitart, F.: The ERA-Interim reanalysis: configuration and performance of the data assimilation system, Q. J. Roy. Meteorol. Soc., 137, 553–597, doi:10.1002/qj.828, 2011. 26178, 26182

Doviak, R. J. and Zrnic, D. S.: Doppler Radar and Weather Observations, Academic Press, San

30 Diego, CA, USA, 1984. 26177

Fritts, D. and Alexander, M. J.: Gravity wave dynamics and effects in the middle atmosphere, Rev. Geophys., 41, 1003, doi:10.1029/2001RG000106, 2003. 26184

Title Page

Abstract	Introduction
Conclusions	References
Tables	Figures

◀ | ▶

◀ | ▶

Back | Close

Full Screen / Esc

Printer-friendly Version

Interactive Discussion

Fritts, D. C. and VanZandt, T. E.: Spectral estimates of gravity wave energy and momentum fluxes. Part I: Energy dissipation, acceleration and constraints, J. Atmos. Sci., 50, 3685–3694, 1993. 26184

Gage, K. S.: Evidence for a $k^{-5/3}$ law inertial range in mesoscale two-dimensional turbulence, J. Atmos. Sci., 36, 1950–1954, 1979. 26184

Gage, K. S. and Green, J. L.: Tropopause detection by partial specular reflection with very high frequency radar, Science, 203, 1238–1240, 1979. 26176, 26177

Gage, K. S. and Green, J. L.: An objective method for the determination of tropopause height from VHF radar observations, J. Appl. Meteor., 21, 1150–1154, 1982. 26176

Gage, K. S., Balsley, B. B., and Green, J. L.: Fresnel scattering model for the specular echoes observed by VHF radar, Radio Sci., pp. 1447–1453, 1981. 26177

Gettelman, A., Hoor, P., Pan, L. L., Randel, W. J., Hegglin, M. I., and Birner, T.: The extratropical upper troposphere and lower stratosphere, Rev. Geophys., 49, RG3003, doi:10.1029/2011RG000355, 2011. 26174, 26175

Hall, C. M., Röttger, J., Kuyeng, K., Sigernes, F., Claes, S., and Chau, J.: First results of the refurbished SOUSY radar: Tropopause altitude climatology at 78° N, 16° E, 2008, Radio Sci., 44, RS5008, doi:10.1029/2009RS004144, 2009. 26176

Hall, C. M., Hansen, G., Sigernes, F., and Kuyeng Ruiz, K. M.: Tropopause height at 78° N 16° E: average seasonal variation 2007–2010, Atmos. Chem. Phys., 11, 5485–5490, doi:10.5194/acp-11-5485-2011, 2011. 26176

Heggelin, M. I., Boone, C. D., Manney, G. L., and Walker, K. A.: A global view of the extratropical tropopause transition layer from Atmospheric Chemistry Experiment Fourier Transform Spectrometer O_3, H_2O and CO, J. Geophys. Res., 114, D00B11, doi:10.1029/2008JD009984, 2009. 26175

Hocking, W. K., Carey-Smith, T., Tarasick, D. W., Argall, P. S., Strong, K., Rochon, Y., Zawadzki, I., and Taylor, P. A.: Detection of stratospheric ozone intrusions by windprofiler radars, Nature, 450, 281–284, doi:10.1038/nature06312, 2007. 26175, 26180

Holton, J. R., Haynes, P. H., McIntyre, M. E., Douglass, A. R., Rood, R. B., and Pfister, L.: Stratosphere-troposphere exchange, Rev. Geophys., 33, 403–439, 1995. 26175

Hooper, D. A. and Arvelius, J.: Monitoring of the Arctic winter tropopause: A comparison of radiosonde, ozonesonde and MST radar observations, in: 9th international workshop on technical and scientific aspects of MST radar, Sci. Comm. on Sol. Terr. Phys., Toulouse, France, 2000. 26176, 26177

Antarctic radar tropopause

S. P. Alexander et al.

Title Page

Abstract	Introduction
Conclusions	References
Tables	Figures

| ◄◄ | ►► |
| ◄ | ► |

Back | Close

Full Screen / Esc

Printer-friendly Version

Interactive Discussion

Hooper, D. A., Nash, J., Oakley, T., and Turop, M.: Validation of a new signal processing scheme for the MST radar at Aberystwyth, Ann. Geophys., 26, 3253–3268, doi:10.5194/angeo-26-3253-2008, 2008. 26176

Hoskins, B. J., McIntyre, M. E., and Robertson, A. W.: On the use and significance of isentropic potential vorticity maps, Q. J. Roy. Meteor. Soc., 111, 877–946, 1985. 26175

Lucas, C., May, P. T., and Vincent, R. A.: An algorithm for the detection of fronts in wind profiler data, Weather Forecast., 16, 234–247, 2001. 26177

May, P. T., Yamamoto, M., Fukao, S., Sato, T., Kato, S., and Tsuda, T.: Wind and reflectivity fields around fronts observed with a VHF radar, Radio Sci., 26, 1245–1249, 1991. 26177

Morris, R. J., Murphy, D. J., Vincent, R. A., Holdsworth, D. A., Klekociuk, A. R., and Reid, I. M.: Characteristics of the wind, temperature and PMSE field above Davis, Antarctica, J. Atmos. Sol. Terr. Phys., 68, 418–435, 2006. 26177

Nastrom, G. D., Green, J. L., Peterson, M. R., and Gage, K. S.: Tropopause folding and the variability of the tropopause height as seen by the Flatland VHF radar, J. Appl. Meteor., 28, 1271–1281, 1989. 26176, 26177, 26183

Pan, L. L. and Munchak, L. A.: Relationship of cloud top to the tropopause and jet structure from CALIPSO data, J. Geophys. Res., 116, D12201, doi:10.1029/2010JD015462, 2011. 26185

Pan, L. L., Randel, W. J., Gille, J. C., Hall, W. D., Nardi, B., Massie, S., Yudin, V., Khosravi, R., Konopka, P., and Tarasick, D.: Tropospheric intrusions associated with the secondary tropopause, J. Geophys. Res., 114, D10302, doi:10.1029/2008JD011374, 2009. 26175

Randel, W. J. and Wu, F.: The polar summer tropopause inversion layer, J. Atmos. Sci., 67, 2572–2581, doi:10.1175/2010JAS3430.1, 2010. 26179, 26182, 26185, 26186

Randel, W. J., Wu, F., and Forster, P.: The extratropical tropopause inversion layer: global observations with GPS data, and a radiative forcing mechanism, J. Atmos. Sci., 64, 4489–4496, 2007. 26182, 26185, 26186

Rao, T. N., Arvelius, J., and Kirkwood, S.: Climatology of tropopause folds over a European Arctic station (Esrange), J. Geophys. Res., 113, D00B03, doi:10.1029/2007JD009638, 2008. 26183, 26186

Reid, H. J. and Vaughan, G.: Convective mixing in a tropopause fold, Q. J. R. Meteorol. Soc., 130, 1195–1212, doi:10.1256/qj.03.21, 2004. 26175, 26183

Sato, K., Watanabe, S., Kawatani, Y., Tomikawa, Y., Miyazaki, K., and Takahashi, M.: On the origins of mesospheric gravity waves, Geophys. Res. Lett., 36, L19801, doi:10.1029/2009GL039908, 2009. 26187

Title Page

Abstract | Introduction

Conclusions | References

Tables | Figures

◄ | ►|

◄ | ►

Back | Close

Full Screen / Esc

Sprenger, M., Maspoli, M. C., and Wernli, H.: Tropopause folds and cross-tropopause exchange: a global investigation based upon ECMWF analyses for the time period March 2000 to February 2001, J. Geophys. Res., 108, 8518, doi:10.1029/2002JD002587, 2003. 26175, 26186, 26188

Sprenger, M., Wernli, H., and Bourqui, M.: Stratosphere–troposphere exchange and its relation to potential vorticity streamers and cutoffs near the extratropical tropopause, J. Atmos. Sci., 64, 1587–1603, doi:10.1175/JAS3911.1, 2007. 26175

Stohl, A., Bonasoni,P., Cristofanelli, P., Collins, W., Feichter, J., Frank, A., Forster, C., Gerasopoulos, E., Gaggeler,H., James, P., Kentarchos, T., Kromp-Kolb, H., Kruger, B., Land, C., Meloen, J., Papayannis, A., Priller, A., Seibert, P., Sprenger, M., Roelofs, G. J., Scheel, H. E., Schnabel, C., Siegmund, P., Tobler, L., Trickl, T., Wernli, H., Wirth, V., Zanis, P., and Zerefos, C.: Stratosphere-troposphere exchange: a review, and what we have learned from STACCATO, J. Geophys. Res., 8516, doi:10.1029/2002JD002490, 2003. 26175

Tomikawa, Y., Nishimura, Y., and Yamanouchi, T.: Characteristics of tropopause and tropopause inversion layer in the polar region, Sci. Online Lett. Atmos., 5, 141–144, doi:10.2151/sola.2009-036, 2009. 26175, 26178, 26182, 26185

Tsuda, T., May, P. T., Sato, T., Kato, S., and Fukao, S.: Simultaneous observations of reflection echoes and refractive index gradient in the troposphere and lower stratosphere, Radio Sci., 23, 655–665, 1988. 26177

Valkonen, T., Vihma, T., Kirkwood, S., and Johansson, M.: Fine-scale modelling simulation of gravity waves generated by Basen nunatak in Antarctica, Tellus, 62A, 319–332, 2010. 26176

Vaughan, G. and Timmis, C.: Transport of near-tropopause air into the lower midlatitude stratosphere, Q. J. R. Meteor. Soc., 124, 1559–1578, 1998. 26175

Vaughan, G. and Worthington, R. M.: Break-up of a stratospheric streamer observed by MST radar, Q. J. R. Meteor. Soc., 126, 1751–1769, 2000. 26183

Vaughan, G., Howells, A., and Price, J. D.: Use of MST radars to probe the mesoscale structure of the tropopause, Tellus, 47A, 759–765, 1995. 26176, 26177

Vincent, R. A. and Eckermann, S. D.: VHF radar observations of mesoscale motions in the troposphere: evidence for gravity wave Doppler shifting, Radio Sci., 25, 1019–1037, 1990. 26184

Wernli, H. and Sprenger, M.: Identification and ERA-15 climatology of potential vorticity streamers and cutoffs near the extratropical tropopause, J. Atmos. Sci., 64, 1569–1586, doi:10.1175/JAS3912.1, 2007. 26175

Antarctic radar tropopause

S. P. Alexander et al.

Title Page

Abstract	Introduction
Conclusions	References
Tables	Figures

◄◄   ►►

◄   ►

Back   Close

Full Screen / Esc

Printer-friendly Version

Interactive Discussion

Wilcox, L. J., Hoskins, B. J., and Shine, K. P.: A global blended tropopause based on ERA data. Part I: Climatology, Q. J. Roy. Meteor. Soc., 138, 561–575, 2011. 26175, 26185

Wirth, V.: Thermal versus dynamical tropopause in upper-tropospheric balanced flow anomalies, Q. J. Roy. Meteor. Soc., 299–317, 2000. 26186

Wirth, V.: Cyclone–anticyclone asymmetry concerning the height of the thermal and the dynamical tropopause, J. Atmos. Sci., 58, 26–37, 2001. 26186

Wirth, V.: Static stability in the extratropical region, J. Atmos. Sci., 60, 1395–1409, 2003. 26185

World Meteorological Organization: Meteorology – a three-dimensional science: Second session of the Commission for Aerology, WMO Bulletin, IV, 134–138, Paris, France, 1957. 26178

Yamamoto, M. K., Oyamatsu, M., Horinouchi, T., Hashiguchi, H., and Fukao, S.: High time resolution determination of the tropical tropopause by the equatorial atmosphere radar, Geophys. Res. Lett., 30, 2094, doi:10.1029/2003GL018072, 2003. 26187

Zängl, G. and Hoinka, K. P.: The tropopause in the polar regions, J. Climate, 14, 3117–3139, 2001. 26175, 26184, 26185

S. P. Alexander et al.

Title Page

Abstract | Introduction

Conclusions | References

Tables | Figures

◄ | ►

◄ | ►

Back | Close

Full Screen / Esc

Printer-friendly Version

Interactive Discussion

Table 1. Radar parameters used in the experiment.

Parameter	Setting
Beam direction	Vertical
Pulse Repetition Frequency	1040 Hz
Coherent Integrations	32
Range	2.0–15.2 km
Range resolution	300 m
Sampling rate	8 min

Antarctic radar tropopause

S. P. Alexander et al.

Title Page

Abstract | Introduction

Conclusions | References

Tables | Figures

◄ | ►

◄ | ►

Back | Close

Full Screen / Esc

Printer-friendly Version

Interactive Discussion
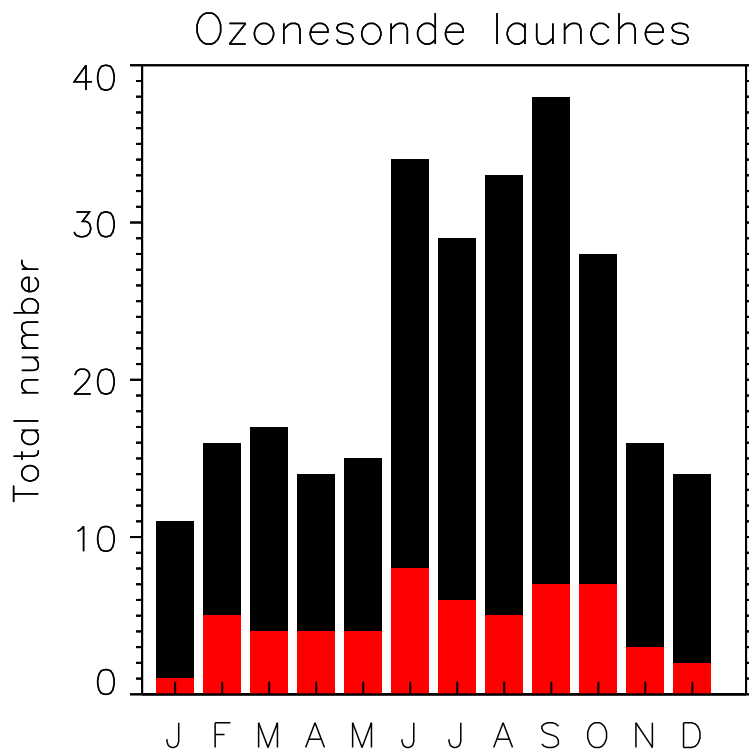
Fig. 1. Distribution of the total number of ozonesonde launches at Davis for September 2009–August 2011 (red colourbars) and February 2003–April 2012 (black colourbars).

Title Page

Abstract | Introduction

Conclusions | References

Tables | Figures

|◀ | ▶|

◀ | ▶

Back | Close

Full Screen / Esc

Printer-friendly Version

Interactive Discussion

Antarctic radar tropopause

S. P. Alexander et al.
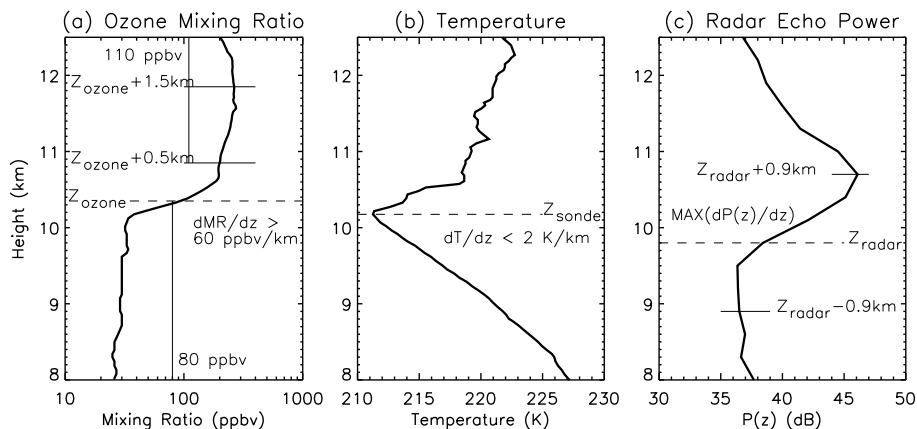
Fig. 2. Example vertical profiles of **(a)** ozone mixing ratio, **(b)** temperature and **(c)** radar echo power (smoothed over three range gates) on 19 March 2010. The dashed horizontal lines on each panel indicate the tropopause height determined with each method. Other annotations illustrate the tropopause detection algorithms which are described in the text.

Antarctic radar tropopause

S. P. Alexander et al.
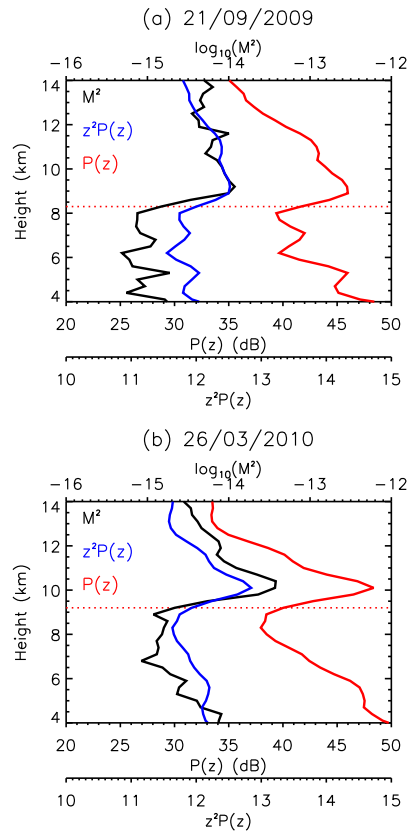
Fig. 3. Radiosonde M^2 (black line), radar power $P(z)$ (red line) and radar range-weighted power $z^2P(z)$ (blue line) on **(a)** 21 September 2009 and **(b)** 26 March 2010. The radiosonde M^2 is interpolated to the radar's height resolution. The horizontal red dotted lines indicate z_{radar}. All profiles are smoothed vertically over three range gates.

Fig. 4. September 2009 (top) and March 2010 (bottom) radar power (dB, colour scale), z_{sonde} (red crosses), z_{ozone} (red circles) and z_{radar} (small black circles). The thin grey line indicates the ERA-Interim 2 PVU geometric altitude at 12 h resolution. Times of missing radar data are marked white and x-axis tickmarks indicate midnight UT.
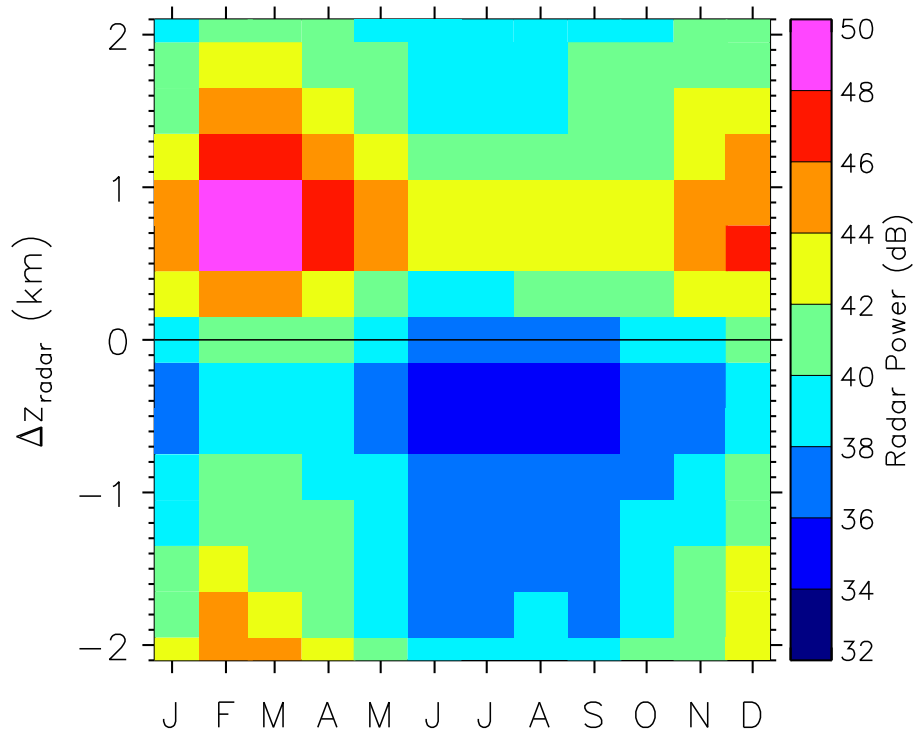
Fig. 5. The monthly mean z_{radar} tropopause-relative radar power (dB). x-axis tickmarks indicate the middle of each month.
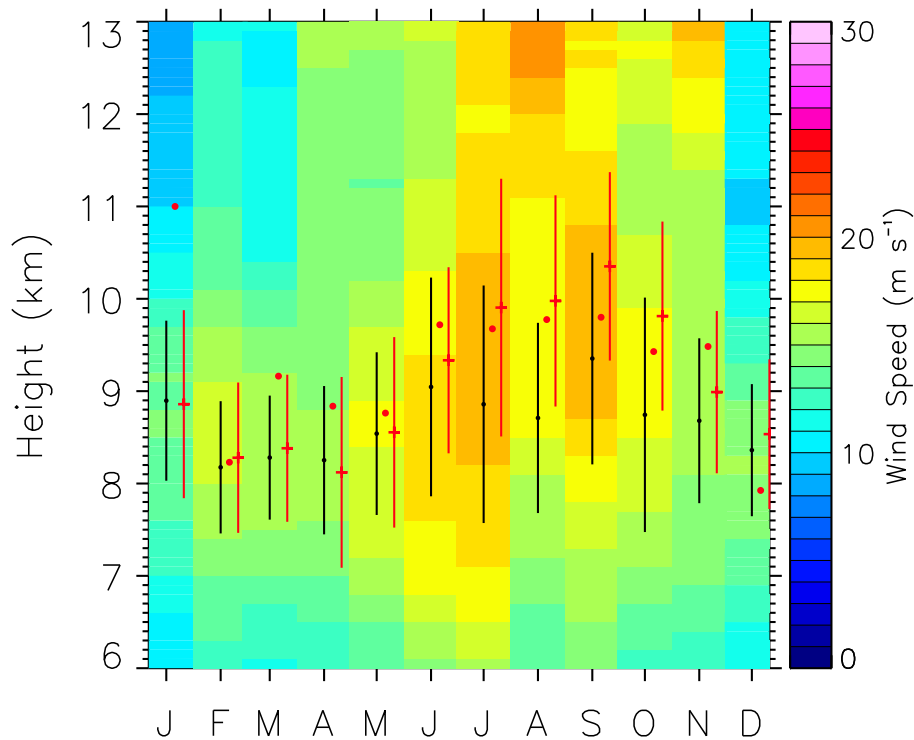
Fig. 6. The monthly mean and standard deviations of z_r (black circles), z_s (red crosses, offset by +10 days), z_o (red circles, offset by +5 days, no standard deviations for clarity) and radiosonde horizontal wind speed (colour, units m s^{-1}) for September 2009–August 2011. x-axis tickmarks indicate the middle of each month.
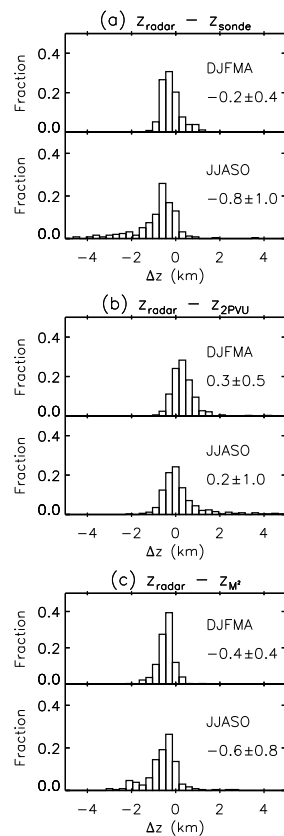
Fig. 7. DJFMA and JJASO distributions of the differences between z_{radar} and **(a)** z_{sonde}; **(b)** z_{2PVU}; and **(c)** z_{M^2}. The seasonal means and standard deviations are given in each panel.

Title Page

Abstract | Introduction

Conclusions | References

Tables | Figures

◀ | ▶

◀ | ▶

Back | Close

Full Screen / Esc

Printer-friendly Version

Interactive Discussion
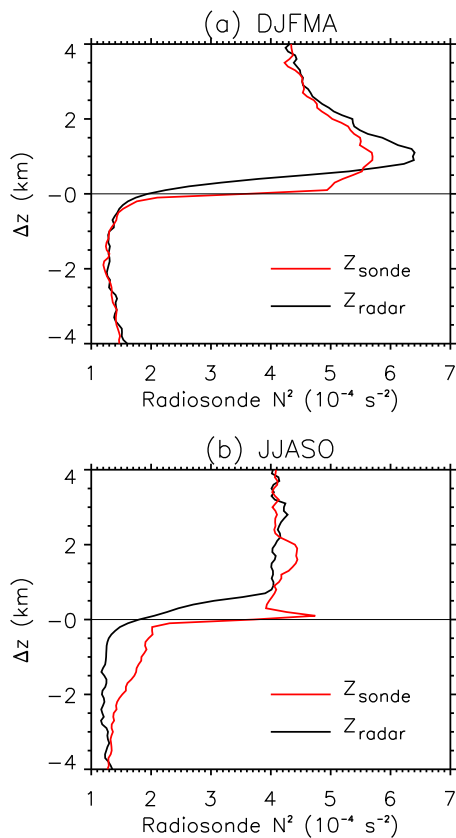
Fig. 8. The tropopause relative profiles of radiosonde N^2 during **(a)** DJFMA and **(b)** JJASO in z_{sonde} (red) and z_{radar} (black) co-ordinates.

Title Page

Abstract | Introduction

Conclusions | References

Tables | Figures

|◄ | ►|

◄ | ►

Back | Close

Full Screen / Esc

Printer-friendly Version

Interactive Discussion
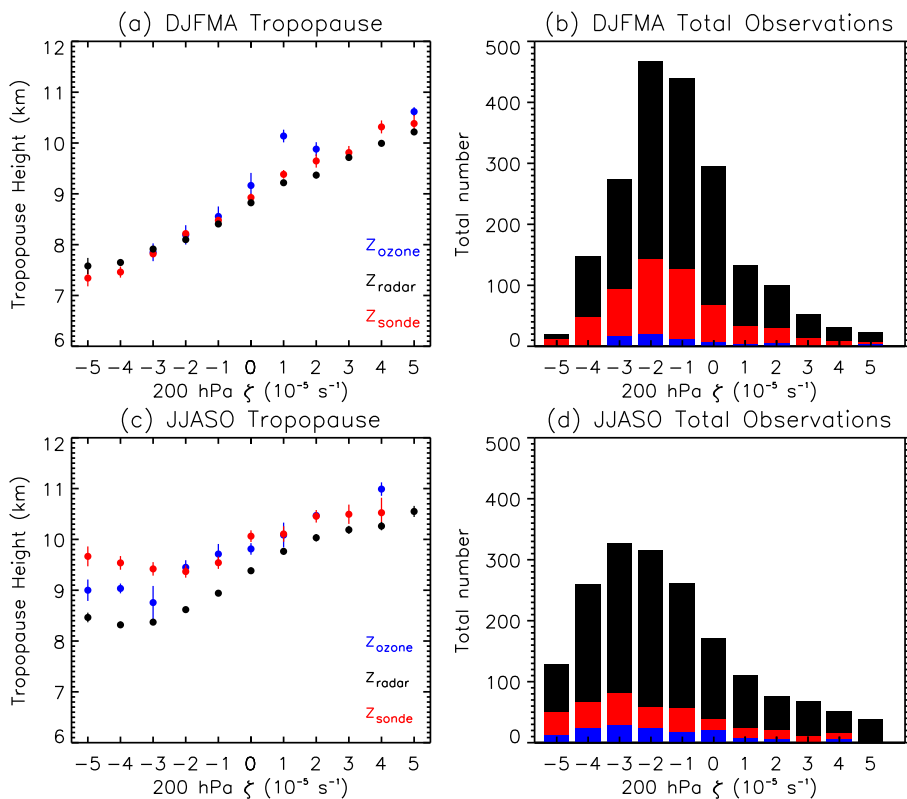
Fig. 9. The mean and standard errors of z_{sonde} (red), z_{radar} (black) and z_{ozone} (blue) as a function of ERA-Interim 200 hPa ζ for **(a)** DJFMA and **(c)** JJASO. Distribution of ζ for the times of observation of z_{sonde} (red), z_{radar} (black) and z_{ozone} (blue) during **(b)** DJFMA and **(d)** JJASO.

Title Page

Abstract | Introduction

Conclusions | References

Tables | Figures

◂◂ | ▸▸

◂ | ▸

Back | Close

Full Screen / Esc

Printer-friendly Version

Interactive Discussion
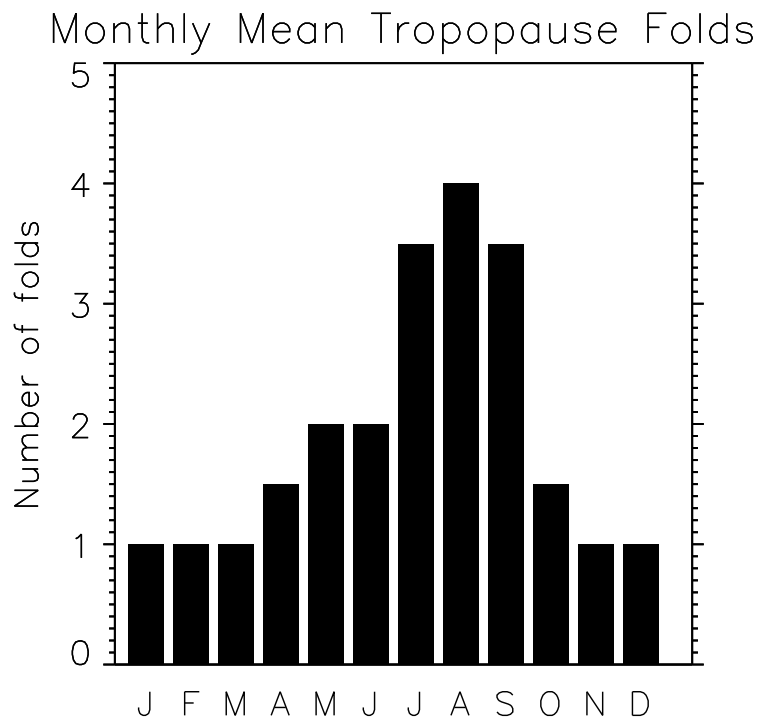
Fig. 10. The monthly mean number of folds during September 2009–August 2011.
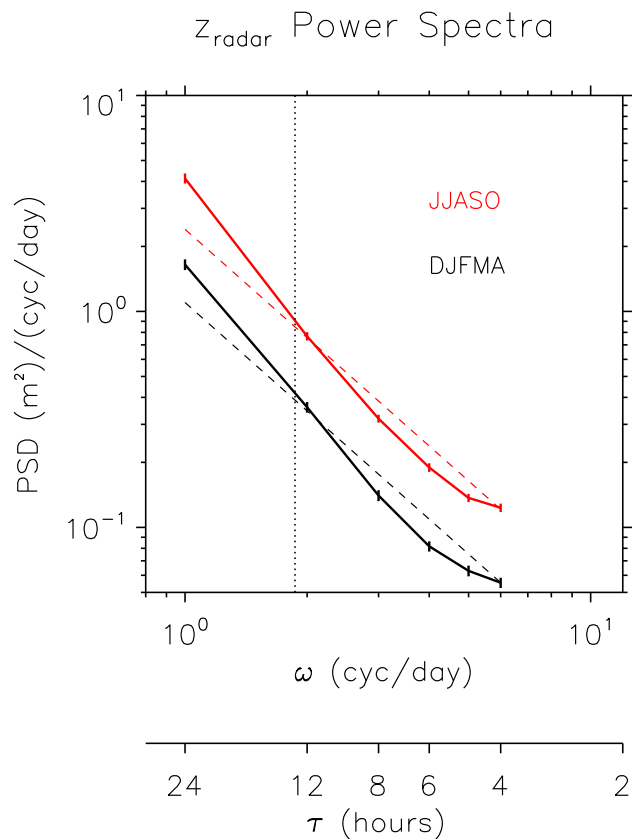
Fig. 11. The z_{radar} power spectral density (PSD) for DJFMA 2010–2011 (black) and JJASO 2010 (red). Standard errors are marked by the vertical bars. Dashed arbitrary lines have gradients of $-\frac{5}{3}$. The vertical dotted line indicates the inertial period at Davis.